q-EELS

Håkon Kvernmoen

June 2021

1 Quick setup

1.1 Joint density of state

Using data from band structures we will try to calculate the q-resolved joint density of state (JDOS). Mathematically this can be written as.

$$J(\omega, q) = \sum_{knn'} \delta(\hbar\omega - (E_{k+q,n'} - E_{k,n})) \tag{1}$$

Here $h\omega$ is the energy difference between a VB and CB. $E_{k,n}$ is the energy at a VB, while $E_{k+q,n'}$ is the energy at a CB, with an additional momentum change between the two states (continuous in k). $q = 0$ would correspond to a direct transition between a valance band (VB) and a conduction band (CB), while $q \neq 0$ allows for indirect transitions. The delta function here gives 1 where the transition corresponds to a specific energy difference $\hbar\omega$ and momentum change q. The sum is over every possible transition, thus effectively representing a count of all transition as a function of ω and q.

1.2 Distribution of states

Temperature can affect the distribution of energy states. Electrons being Fermions, the distribution will follow the Fermi-Dirac statistic. The probability of an available state being occupied as a function of energy then follows:

$$f(E) = \frac{1}{1 + e^{(E-E_f)/k_B T}} \tag{2}$$

Where k_B is the Boltzmann constant and T the temperature. E_f is the Fermi-energy and decides the energy level where half of the available states are occupied by an electron. For semiconductors the Fermi-energy lies in the band gap, thus making the VB highly populated with electrons, while the CB contains few. Initially we will look at transitions happening at absolute zero. Thus for the VB all states will be occupied by an electron, $E - E_f < 0 \Rightarrow f(E)_{T=0} = 1$ and for the CB all states will be empty, $E - E_f > 0 \Rightarrow f(E)_{T=0} = 0$.

1.3 Approach

In the following we will create data based on idealised bands. Modeling VBs and CBs using different functions, we can try to understand how different shapes and parameters affect the resulting JDOS. Bands will be created in some region of linearly spaced k-vectors. Since we have set $T = 0$, every state in the VB will be occupied and every state in the CB will be empty. Thus, to calculate every possible transition we consider a k point in the VB k_i, corresponding to an energy E_i. Thereafter we calculate the energy and momentum change between the VB point and every CB point giving $\Delta E_{ij} = E_i - E_j$, $q_{ij} = k_i - k_j$. This is done for every VB point i, giving $n_{VB} \cdot n_{CB}$ transitions, where n_{VB} and n_{CB} is the number of k-points in the VB and CB respectively. To calculate the intensity from Equation 1, we have to define an energy and momentum bin size. This decides how similar two sets of ΔE's and q's are before they are considered equal. This will be noted δq and δE.

2 Simplified band structure models

We will here look at simplified models for 1-dimensional bands. Introduction-wise we will look at transitions between parabolic valence bands (VBs) and conduction bands (CBs). We can then test our calculation against the an analytical result for the 1-dimensional JDOS at $q = 0$. Thereafter more complex structures will be studied where pertubations are added to the parabolic bands, moving the Fermi energy and multiple band transitions.

2.1 Direct gaps

We will first consider one of the simplest possible models, completely parabolic bands. This is not a very realistic representation, but serves as a simple introduction to understand both JDOS plots and code development. Parabolic bands can approximate band structures at the top of the VB and bottom of the CB [1]. With some constant energy, the energy as a function of wave vectors becomes.

$$E(k) = \frac{\hbar^2 k^2}{2m^*} + E_0 \tag{3}$$

Where E_0 is a constant giving the edge of a band. Band minimums and maximums will be placed at different k values, simply translated by $k' = k + k_0$. m^* is the *effective mass* of the electron and a smaller m^* would result in a sharper band peak/valley and a larger m^* a less steep peak/valley. [1] also states that the effective mass of VBs are negative, thus giving the characteristics band structure. Alternatively one can argue this through the Virial theorem [2]. Electrons in the conduction band are not predominantly bound by one nucleus, but electrons in the valence bands are. For an inverse square force (as the Coulomb potential is) we know that the average potential energy of the electron is twice that of the kinetic energy with a negative sign. The CBs and VBs will respectively be regarded as.

$$E_c(k) = E_{0,c} + \frac{\hbar^2 k^2}{2m_c^*} \qquad \text{and} \qquad E_v(k) = E_{0,v} - \frac{\hbar^2 k^2}{2m_v^*} \tag{4}$$

Where m_v^* is implied to be positive. This will form the basis for our introductory models.

2.1.1 Analytical JDOS

To test our algorithm, comparing with analytical results serves as an important benchmark. For our simplified band structure model (presented later), we will look at 1-dimensional bands. We then aim to calculate the theoretical JDOS for parabolic 1-dimensional bands for $q = 0$ to serve as an assessment of our calculations. From [3] we express the volume Ω_n of an n-dimensional k-space as.

$$\Omega_n(k) = c_n k^n \tag{5}$$

Where c_n is the length/area/volume of the n-dimensional unit sphere, where k is the maximum allowed wave vector. For our 1-dimensional model, the length on the unit sphere is $c_1 = 2$ [4]. The number of possible energies E inside an interval $[E, E + \mathrm{d}E]$, the density of state, then follows as.

$$D_n(E) = \frac{\mathrm{d}\Omega_n(E)}{\mathrm{d}E} \tag{6}$$

In general every transition between the VB and CB can result in a momentum change between two states. Thus we consider a state in the VB with an initial wave vector k_i, with a transition to a CB state with momentum k_f. We call the wave vector transfer between the two states $q = k_f - k_i$. By conservation of momentum the two parabolic bands in eq. (4) becomes.

$$\hbar k_i = \hbar k_f + \hbar q$$

$$E_c(k_i) = E_{0,c} + \frac{\hbar^2 (k_i - q)^2}{2m_c^*} \qquad \text{and} \qquad E_v(k_i) = E_{0,v} - \frac{\hbar^2 k_i^2}{2m_v^*}$$

The energy difference between the CB and VB thus becomes.

$$E_c(k_i) - E_v(k_i) = E_{0,c} + \frac{\hbar^2 (k_i + q)^2}{2m_c^*} - \left(E_{0,v} - \frac{\hbar^2 k_i^2}{2m_v^*} \right) \tag{7}$$

Considering the case of direct transitions ($q = 0$), we rename $k_i \to k$ as it is an arbitrary k-vector, defining the lowest energy transition (band gap) $E_g = E_{0,c} - E_{0,v}$, with other energy transitions as $E = E_c(k) - E_v(k)$. In addition by defining a 'mean' effective mass $m_\mu^* = m_c^* m_v^* / (m_c^* + m_v^*)$, eq. (7) becomes.

$$E - E_g = \frac{\hbar^2 k^2}{2m_\mu^*} \tag{8}$$

Finally, by solving this equation for k, we can insert it into the volume of the k-space from eq. (5) with $c_n = 2$ and acquire the JDOS by taking the energy derivative in eq. (6)

$$k = \frac{\sqrt{2m_\mu^*(E - E_g)}}{\hbar}$$
$$D(E) = \frac{\mathrm{d}}{\mathrm{d}E}\left(2 \cdot \frac{\sqrt{2m_\mu^*(E - E_g)}}{\hbar}\right) = \frac{\sqrt{2m_\mu^*}}{\hbar}(E - E_g)^{-\frac{1}{2}} \tag{9}$$

2.1.2 Computation and testing

We begin with a simple direct band gap of $E_g = 1$ eV. For simplicity we make both bands symmetric around $k_0 = 0.5$ Å^{-1}with the same effective mass $m^* = 0.5m_e$. Both the band diagram and the resulting JDOS can be seen in Figure 1

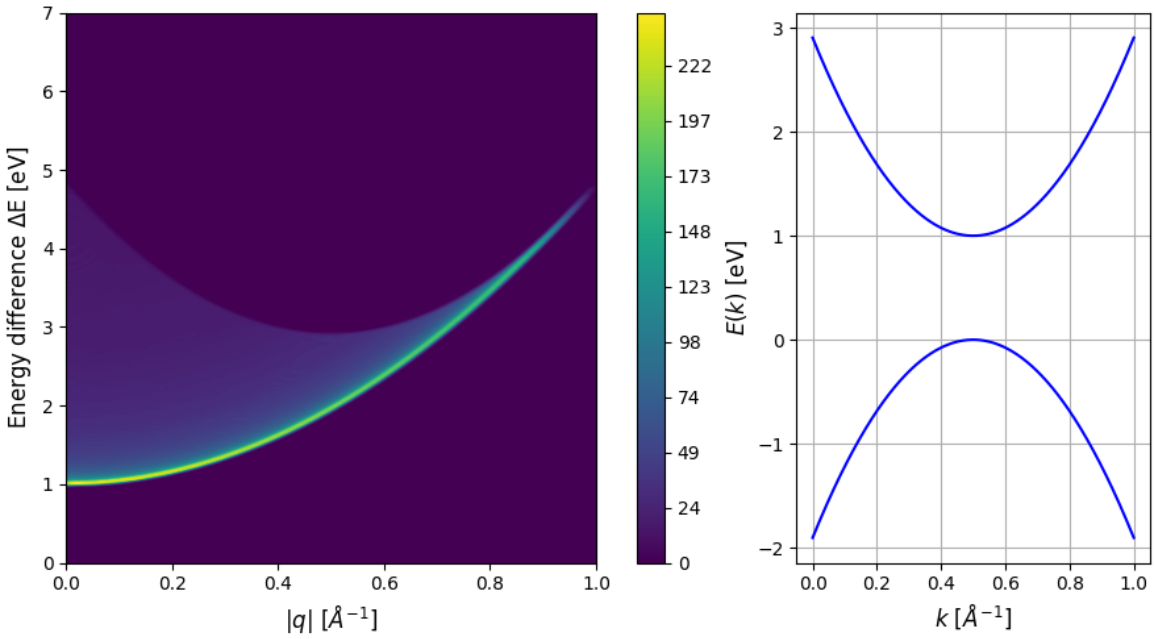

Figure 1: Right: The direct parabolic band gap plotted on $k \in [0, 1]$Å^{-1} centered at $k_0 = 0.5$Å^{-1}, both with $m^* = 0.5m_e$ and a band gap set to $E_g = 1$ eV. Left: The corresponding JDOS plot, showing the amount of transitions as a function of absolute momentum transfer and energy difference. Produced with a energy and momentum bin sizes of $\delta E = 10^{-2}$ eV and $\delta q = 4 \cdot 10^{-3}$ Å^{-1}. Here a Gaussian filter with $\sigma = 0.5$ has been used to smooth out the figure.

Around $\Delta E = 1$ eV, $|q| = 0$ we see the lowest possible energy difference corresponding to the band gap of $E_g = 1$eV. The defining feature is the steadily diminishing yellow/green line starting at $(0, 1$ eV) and ending at $(1$ Å$^{-1}, 5$ eV). With the lack of a more creative mind we will call this a main line. If we imagine starting at a specific point around the top the VB, transition with smaller ΔE will be more abundant than those with larger ΔE, due to the steepness of the CB quickly increasing away from $k_0 = 0.5$Å^{-1}. Moving further down the VB where the steepness increases, both ΔE and $|q|$ w.r.t. the bottom of the CB increases, but again since this part of the CB is quite flat we will get more transitions here than any other areas of the CB. Since the amount of transitions decreases far down the VB to far up the CB we get a fading effect along the main line for higher ΔE and $|q|$.

The less populated area above the main line is also of interest. At $|q| = 0$ we only consider direct transitions (vertical lines between VB and CB). Again the larger population of points around the flatter areas of both the VB and CB consists of more transitions than the steeper parts. Holding $|q|$ constant and considering a line $|q| < 0.5$Å^{-1}(in the JDOS plot), the largest possible energy transition decreases. In the band structure diagram this corresponds a transition line now not being vertical and thus the highest energy transition is smaller. At $|q| > 0.5$ Å^{-1}we allow for a transition from the bottom of the CV to cross $k_0 = 0.5$ Å^{-1}, thus the amount of transitions increases.

It should be stated that these idealized bands are inherently flawed in how states are distributed in the bands. If we take direction of the momentum transfer into account and create the bands on the same k-points, the most common transition will always occur at $q = 0$. In example assume we have two bands both created on $k \in [0, 1]$ Å^{-1}spaced 0.1 Å^{-1}apart. Then we will have 10 transitions for $q = 0$, 9 for each $q = \pm 0.1$ Å^{-1}and so on until only one for each $q = \pm 1$ Å^{-1}. This is the

case for the previous indirect band gap and can be seen in figure Figure 2. When using this approach fading of the JDOS at higher q values is inevitable. Real band structures does not have linearly k-spaced states, so any comparison to real data is qualitative at best.

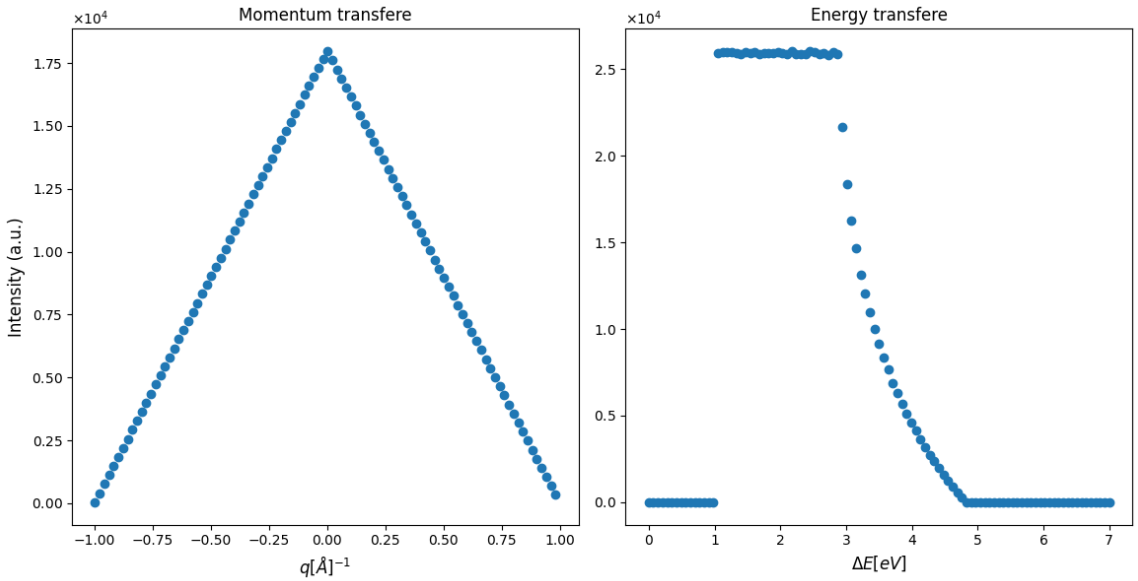

Figure 2: Left: The number of transitions at specific q-values as a fraction of all transitions, integrated over every energy. Right: The number of transitions at specific ΔE-values as a fraction of all transitions, integrated over every momentum transfer. For both figures, only every 20'th point is shown for clarity.

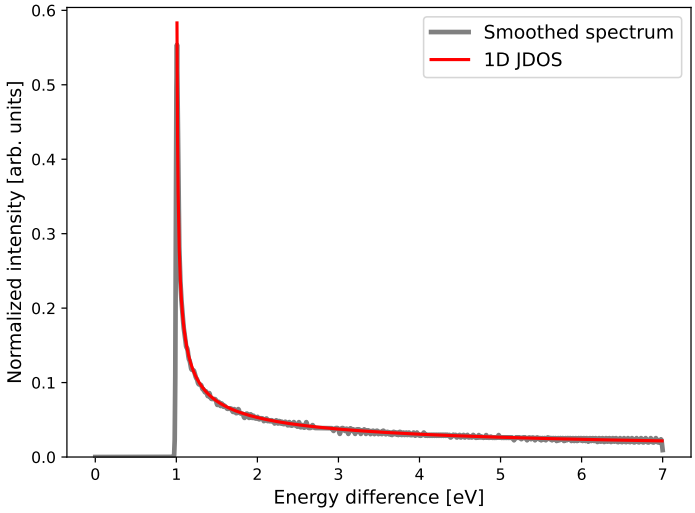

Figure 3: The calculated energy difference spectrum for $q = 0$, fitted wit the analytical 1-dimensional JDOS. The JDOS was calculated with energy and momentum bin sizes at $\delta E = 5 \cdot 10^{-3}$ eV and $\delta q = 2 \cdot 10^{-3}$ Å^{-1}respectively, with a counted energy range at $E \in [0, 7]$ eV. The analytical JDOS was fitted on $E \in [1 + \delta E, 7 - \delta E]$ as bin sizes are halved at the edges. The fit was preformed after the Gaussian filter was applied.

In trying to assess our calculation, we fit the 1-dimensional JDOS as presented in eq. (9). As our data is quantized (counting states) and completely dependent on the amount of k-points as well as energy and momentum bin sizes, the intensity can not be predicted using the prefactor in eq. (9). Thus we will fit the analytical JDOS with the prefactor and band gap as free parameters. We consider the same direct band gap, but now increasing both the sampled k-range to $k \in [-0.5, 1.5]$ Å^{-1}and the energy and momentum bin sizes to $\delta E = 5 \cdot 10^{-3}$ eV and $\delta q = 2 \cdot 10^{-3}$ Å^{-1}respectively. This is done to increase the range of energy transitions allowing more points to fitted, as well as reducing overlap between different q-values. The result is presented in Figure 3. The computed spectrum for $q = 0$ fits very good with the analytical expression, with the band gap coefficient calculated to $E_g = 0.9997$ eV with a coefficient standard deviation of $\sigma_{Eg} = 7.511 \cdot 10^{-9}$ eV. The fitted band gap value deviation from the set band gap of 1 eV is way below the energy bin size. For determining the band gap from this spectrum, fitting a narrower energy range that does not include the diverging peak at $E_g = 1$ eV is preferred, as this will bring some numerical instability to the fit. However the whole range was chosen here as this is an assessment of our model.

2.1.3 Different effective masses

We now move to changing the shape of the CV, thus not making the bands identical. The setup is identical to the last, but now the effective mass of the CB has been halved ($m^* = 0.25 m_e$). This is presented in Figure 4

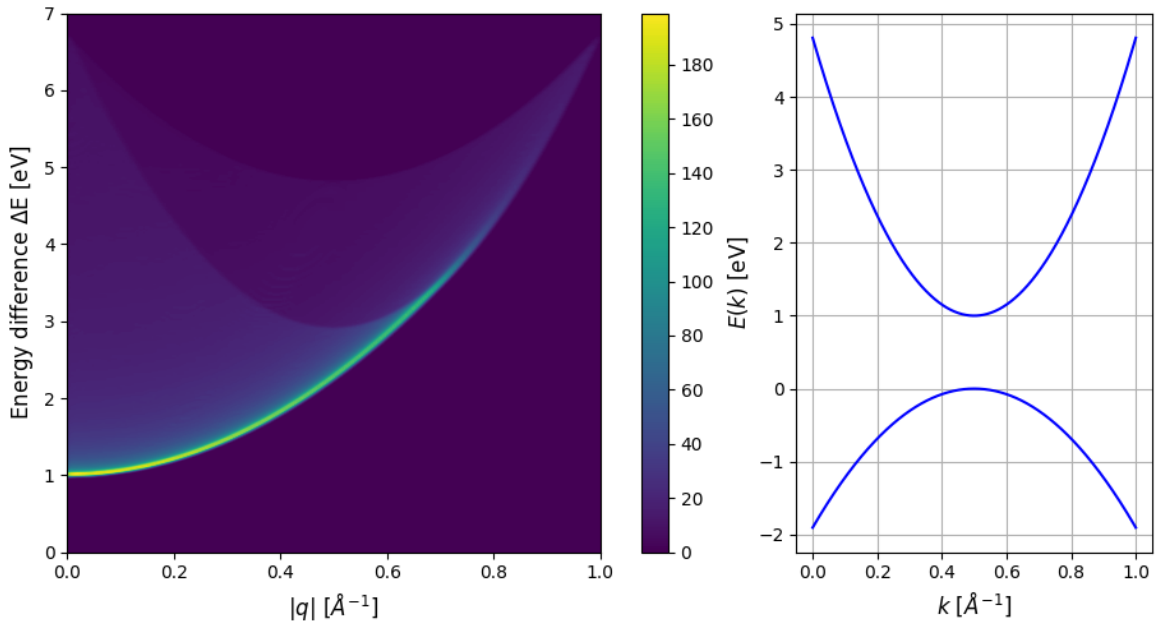

Figure 4: Idential setup as Figure 1, but now the CB has an effective mass of $m^* = 0.25m_e$. Energy and momentum bin sizes has been set to $\delta E = 1.4 \cdot 10^{-2}$ eV and $\delta q = 2 \cdot 10^{-3}$ Å^{-1}. The same Gaussian filter has been used.

The main features are identical to the ones in Figure 1, but with some key differences. Firstly even tough the main line has almost identical shape, it fades away much quicker. This is due to the high $\Delta E/|q|$ transitions becoming rarer due to the increased steepness of the CB. It also reaches farther in terms of ΔE, again attributed to the CB reaching higher energies.

We now also have two distinct less populated areas, with the top one being darker than the bottom one. The bottom one is attributed to transitions from lower down the CV to lower down in the CB. This can be seen by considering the bottom of its parabolic shape, located at $(0.5$ Å$^{-1}, 3$ eV) and considering transitions from the bottom of the VB to the bottom of the CB. The less populated area above corresponds to transitions form the top of the VB to the top of the CB, considering the point $(0.5$ Å$^{-1}, 5$ eV). The bottom area is denser than the top one due to the bottom of the CV being less stead than the top of the CB.

2.2 Indirect gaps

We now move to indirect band gaps. This means that the lowest energy transition will not occur at $q = 0$. Since the two previous band structures have been symmetric around the band gap, we got mirror images for transitions q and $-q$. For further experimentation the direction of the momentum transfer will be present in the JDOS plots.

First we consider a structure where both bands have the same effective mass, $m^* = 0.5m_e$. Still keeping to parabolic bands, we center the CB at $k_{0,c} = 0.8$ Å^{-1}and the VB at $k_{0,v} = 0.4$ Å^{-1}. Keeping the band gap at $E_g = 1$ eV we should see the lowest energy transition at $q_g = k_{0,c} - k_{0,v} = 0.4$ Å^{-1}. The result can be seen in Figure 5.

Again the dominating feature is the lower parabolic band dividing the highly populated region with low energy transitions and the area with no transitions. This is centered around $(0.4$ Å$^{-1}, 1$ eV), correctly identifying the indirect band gap. Even though this is the area with highest intensity, it should be noted that this is not generally the case. However this is the case for this simplified model, most likely attributed to the abundance of points around the flat areas at the top of the VB and the bottom of the CB.

In contrast to the symmetric case from the previous direct gaps, we now have two different main lines. Transitions $q > 0.4$ Å^{-1}(right of the band gap in the JDOS plot) correspond to transitions from the top of the VB to higher up the CB $k \approx 1$ Å^{-1}and upwards. Due to this large momentum transfer the transitions ends up high in the CB (where the states becomes less abundant) and thus fades out at around $q \approx 1.25$ Å^{-1}. On the other hand transitions $q < 0.4$ Å^{-1}(left of the band gap in the JDOS plot) do not require a large momentum transfer. Thus one allows for high energy transitions with low momentum changes and the main line fades slower.

It should be stated that these figures are (not surprisingly) dependent on the energy and momentum bin sizes δE and δq. In Figure 6 one can see the same structure as in Figure 5, but with 5 times larger energy and momentum bin sizes. The bin sizes decides how similar the states has to be before counting them as equal, effectively working as a tolerance for the delta functions in eq. (1). This can also be seen by comparing the intensity colorbar of Figure 5 and Figure 6, where the large bin size figure has higher counts due to more states being considered equal.

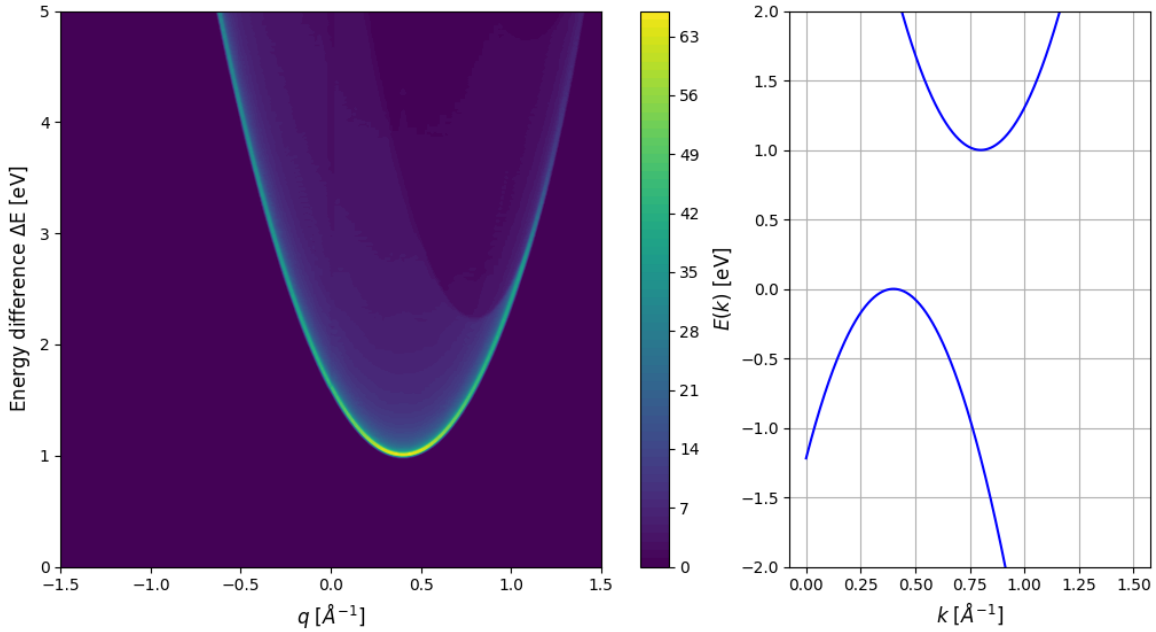

Figure 5: Indirect band gap of parabolic bands with equal effective mass, $m^* = 0.5m_e$. Both bands were samples in $k \in [0, 1.5]$ Å^{-1}. Produced with energy and momentum bin sizes $\delta E = 10^{-2}$ eV and $\delta q = 6 \cdot 10^{-3}$ Å^{-1}. The same Gaussian filter used as in the previous figures.

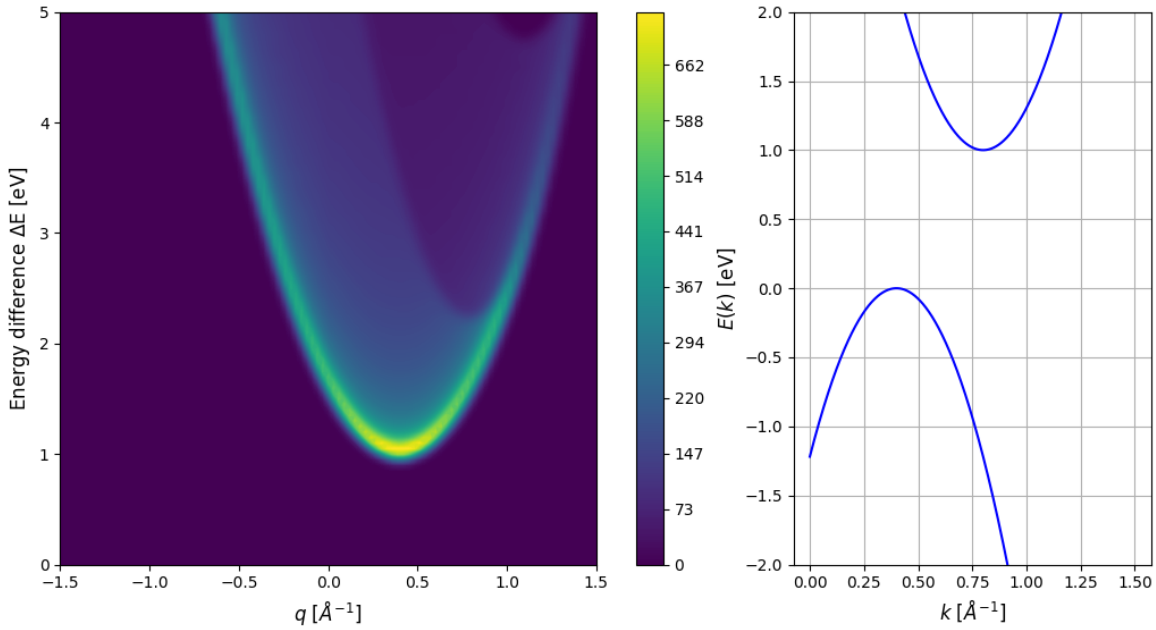

Figure 6: Indirect band gap of parabolic bands with equal effective mass, $m^* = 0.5m_e$. Both bands were samples in $k \in [0, 1.5]$ Å^{-1}. Produced with energy and momentum bin sizes $\delta E = 5 \cdot 10^{-2}$ eV and $\delta q = 3 \cdot 10^{-2}$ Å^{-1}. The same Gaussian filter used as in the previous figures.

2.3 Non-parabolic bands

A slightly more complex model modifies the parabolic structure by α, a constant with units of inverse energy. This can be expressed as

$$E(k)(1 + \alpha E(k)) = \frac{\hbar^2 (k - k_0)^2}{2m^*} \tag{10}$$

Solving the second order equation we find.

$$E(k) = \frac{-1 + \sqrt{1 + \frac{2\alpha\hbar^2(k-k_0)^2}{m^*}}}{2\alpha} + E_0 \tag{11}$$

With E_0 again added to define the edge of the band. This will yield bands that are parabolic close to the minimum and maximum of the CB and VB respectively. Further from the extreme points the flattens out and we obtain a more linear curve.

To see how this "perturbation" effects the JDOS, we change the CB from the last setup to follow eq. (11) with $\alpha = 0.7$ eV^{-1}. This can be seen in Figure 7. There are some differences when compared to the parabolic indirect gap. Firstly the shape of the main line around the indirect band gap (0.4 $\text{Å}^{-1}, 1$ eV) still has the parabolic shape. However when moving away from $q = 0.4$ $\text{Å}^{-1}$the slope change decreases and approaches a linear curve. This is due to transitions reaching higher up in the CB having a smaller ΔE for a specific q compared to the parabolic CB.

The non parabolic band makes the main line fade faster than the case where both bands were parabolic. This however is an effect of the bands only being sampled on the interval $k \in [0, 1.5]$ Å^{-1}(for easier compartment to both bands being parabolic). Increasing the sampling range extends these lines, but due to the CBs linear trend this requires larger momentum transfers.

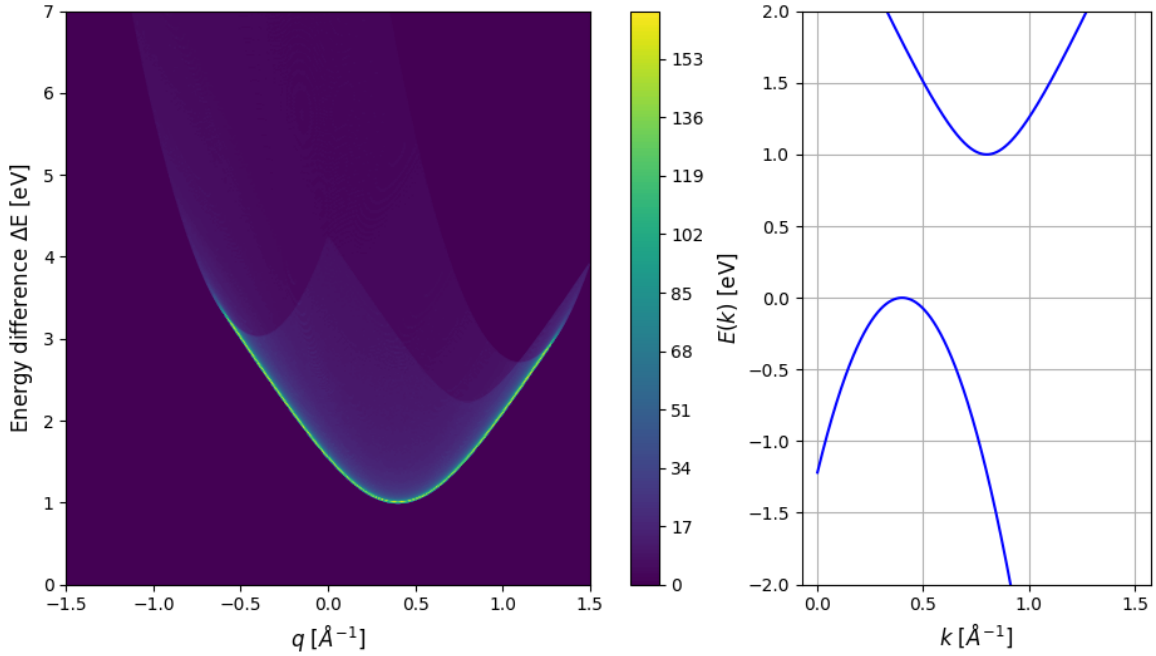

Figure 7: Identical setup as in Figure 5, but with the CB following eq. (11) using $\alpha = 0.7$ eV^{-1}. Energy and momentum bin sizes at $\delta E = 1.4 \cdot 10^{-2}$ eV and $\delta q = 6 \cdot 10^{-3}$ Å^{-1}

2.4 Beyond 2 bands

So far we have only seen transitions from a single VB to a single CB. Semiconductor band structures contain multiple bands, often overlapping, so adding multiple VBs and/or CBs is of interest. Again we begin with a simple example. We add another CB to the indirect band gap from Figure 5 with the same parabolic shape and effective mass with a minimum at $k_{0,c} = 0.6$ Å^{-1}. The two CBs now share a minimum energy at $E_g = 1$ eV located at $k_{0,c} = \{0.6, 0.8\}$ Å^{-1}. Thus we should have two band gaps of $E_g = 1$ eV located at $q_g = \{0.2, 0.4\}$ Å^{-1}.

The resulting band structure and JDOS can be seen in Figure 9, with 'the area of interest' enlarged in Figure 8. Adding another band results in another main line appearing. Similarly with the indirect transition with a singe CB (Figure 5) these lines correspond to transitions from the top of the VB to increasingly higher energies in the CBs (due to the abundance of states at the top of the VB). The two main lines have the parabolic shape mimicking the shape of the bands. The right most line corresponds to transitions to the CB located at $k_{0,c} = 0.8$ Å^{-1}while the left to $k_{0,c} = 0.6$ Å^{-1}. The most common transitions happens at approximately (0.2 $\text{Å}^{-1}, 2.05$ eV). In the band gap diagram this corresponds to the area around the crossing of the bands, where the transition intensity effectively doubles. The fading at $\sim q > 0.8$ Å^{-1}again corresponds the high momentum transfers from the top of the VB to the top right of the two CBs where states of the CBs becomes sparse.

The point where the fading begins is dependent on the k sampling range, but larger ranges only moves this fading to higher energy transitions.

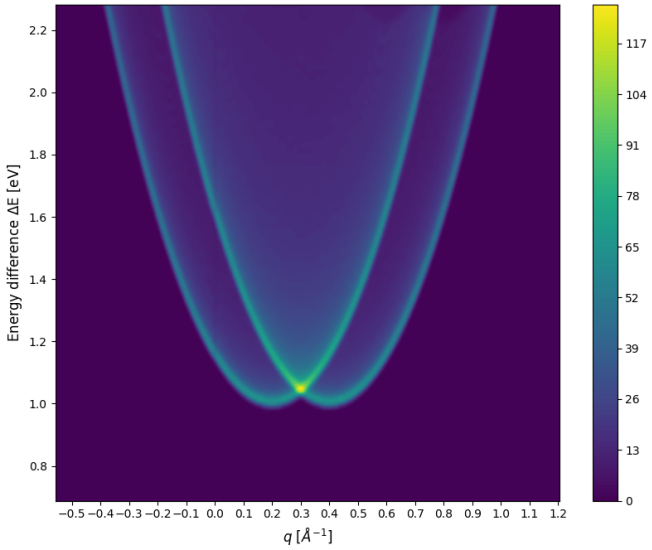

Figure 8: Enlargement of Figure 9 around smallest ΔE and q transitions.

We now take a closer look at the low energy and momentum transitions. The band gaps are correctly identified at $E_g = 1$ eV for momentum transfers 0.2 Å^{-1}and 0.4 Å^{-1}.

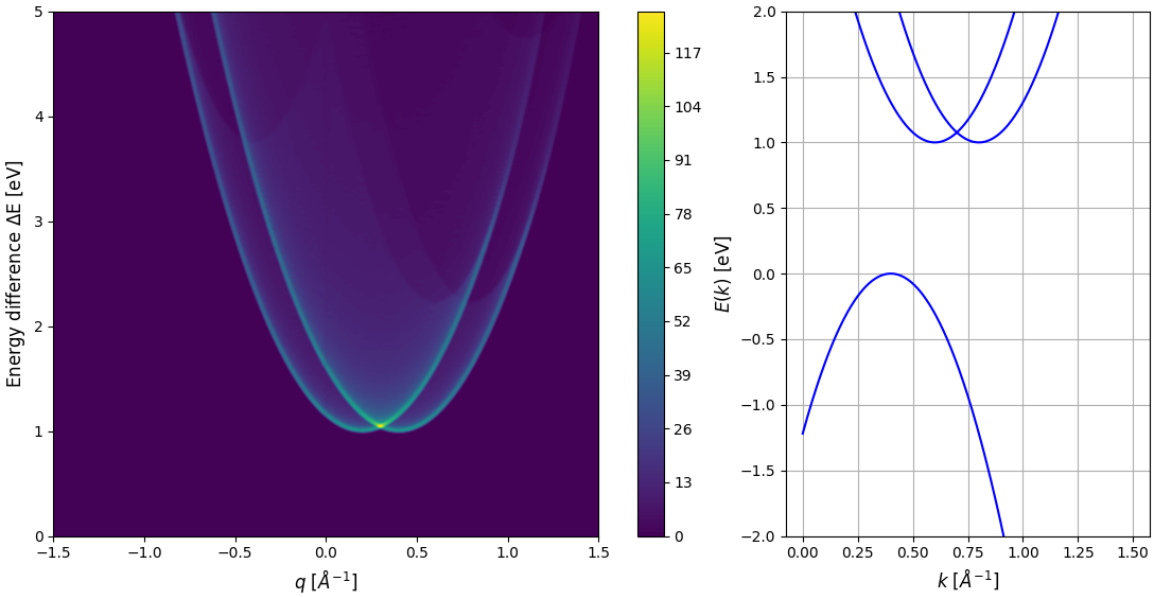

Figure 9: Points sampled from $k \in [0, 1.5]$ Å^{-1}for all 3 bands, with the same effective mass $m^* = 0.5m_e$. VB centered at $k_{0,v} = 0.4$ Å^{-1}and CBs at $k_{0,c} = \{0.6, 0.8\}$ Å^{-1}. For the JDOS we have energy and momentum bin sizes at $\delta E = 10^{-2}$ eV and $\delta q = 6 \cdot 10^{-3}$ Å^{-1}

.

Next we will see how flat bands differs to steeper bands. We consider the same two bands from Figure 1, but at another non-parabolic VB. Setting $\alpha = 5$ eV^{-1}will make sure the band becomes linear when moving away from its maximum value at $k_0 = 0.5$ Å^{-1}. In addition setting a large effective mass $m^* = 5m_e$ will make sure the VB is relatively flat when k moves away from $k_0 = 0.5$Å^{-1}. In addition the VB has a maximum at $E_0 = -0.5$ eV to easier distinguish between the two bands in the JDOS.

The band structure and the resulting JDOS is presented in Figure 10. The steep VB has the same characteristic shape as in figure Figure 1, with a band gap at $(0, 1$ eV$)$. The flat VB has a minimum energy transition at $(0, 1.5$ eV$)$. There is a clear difference of intensity of transitions from the two VBs. This is attributed to the low energy spread between transitions from the flat VB to the CBM. Looking at the band structure and comparing a transition from $(0, \sim -0.6$ eV$)$ and $(0.5$ Å$^{-1}, -0.5$ eV$)$ to the CBM, the energy difference is almost equal, while the momentum transfer spans half the band structure. The steeper VB does not have this feature and thus the possible transitions are more spread out in the JDOS.

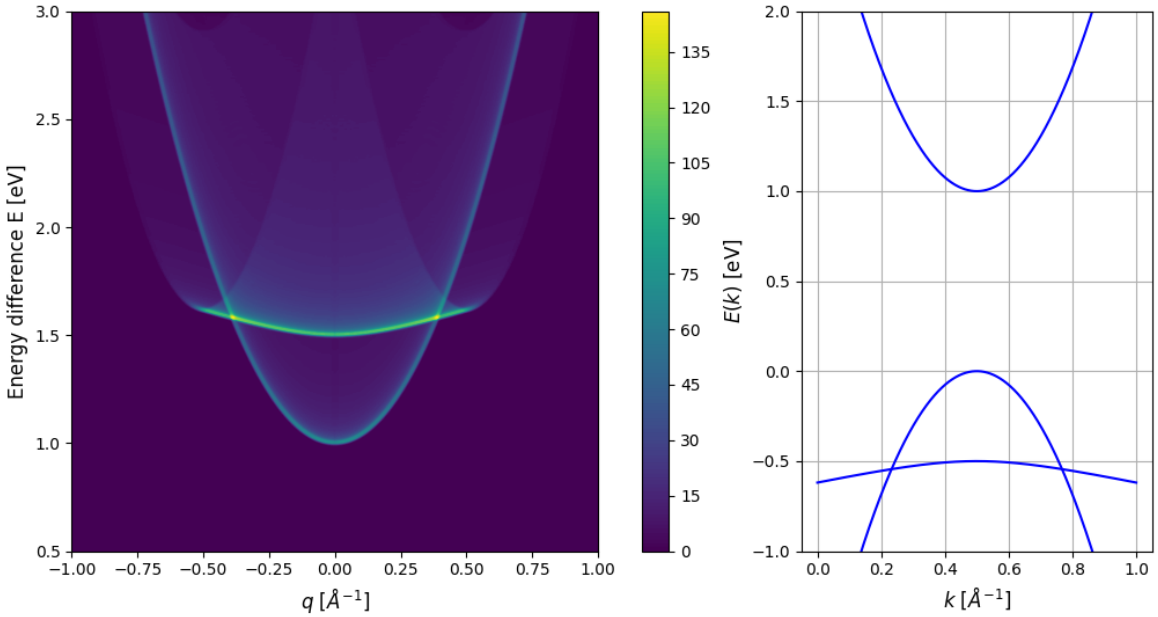

Figure 10: Identical set as in figure Figure 1, but with an additional flat VB added. In addition this is resolved for q transitions in both directions and a narrower energy range is shown.

2.5 Moving the Fermi energy

Optical and electronic properties of semiconductors can be modify by doping the material with small amounts of different elements. This results in two different defects to the material, either adding charge carriers (n-type) or by adding electron holes (p-type). The Fermi energy can be moved towards the CB (n-type) or towards the VB (p-type) [5]. We will here imagine a heavy n-type doping, where the Fermi energy is moved above the CBM. Due to the Fermi energy now being above the CBM, some of the states lower down the CB will be occupied by electrons. Thus the lowest energy transition is no longer the band gap, since very low energy transitions inside the CB is possible. In addition the band gap will be increase, adding a factor of $E_g - E_f$ compared with the Fermi energy being placed between the CB and CV.

We go back to the band structure from Figure 5 and move the Fermi energy to $E_f = 1.25$ eV, seen in figure Figure 12. The resulting JDOS can be seen in Figure 11. As expected the band gap is now moved to $E_g = 1.25$ eV. Compared with the undoped Fermi energy, this transition can happen at two different momentum changes, $q \approx 0.2$ Å^{-1}and $q \approx 0.65$ Å^{-1}. As seen in Figure 8 and Figure 9, this feature seems to be characteristic structures where we have multiple bands. Moving the Fermi energy effectively splits the CB into two partitions (symmetric due to the parabolic structure) mimicking a multi-band structure. There are also some transitions for very low energies, attributed to interband transitions in the CB. Considering these, there are no $q = 0$ transition, thus a small amount of momentum transfer is always required. For transition just above $E = 0$, these can happen by small momentum changes each of the CB partitions separately (the symmetric lines centered at $q = 0$) or between the two partitions (at aroud $q \approx \pm 0.35$ Å^{-1}).

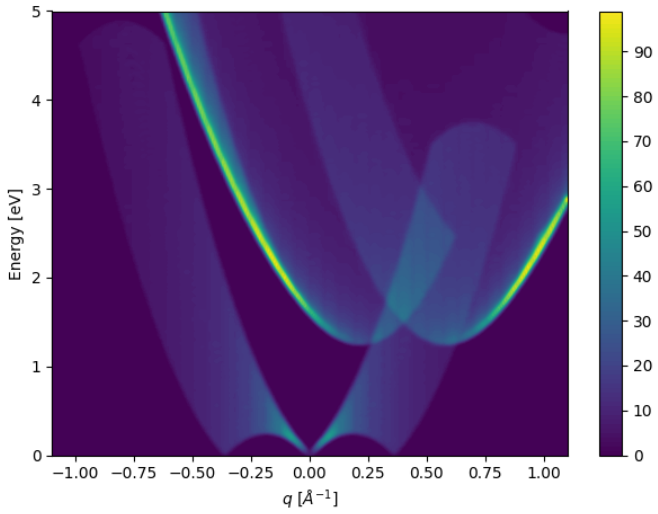

Figure 11: JDOS of the band structure seen in Figure 12. Energy and momentum bin sizes at $\delta E = 2 \cdot 10^{-2}$ eV and $\delta q = 8 \cdot 10^{-3}$ Å^{-1}

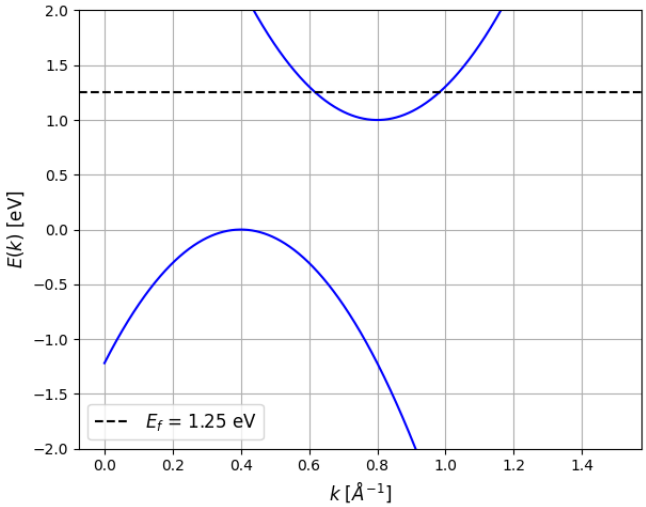

Figure 12: Band structure with the Fermi energy moved to $E_f = 1.25$ eV. Sampled on $k \in [0, 1.5]$ Å^{-1}.

3 Extraction from band structure

Next we will try to recreate some of the features from Schuster et al. [6], to see if some of the same structures can be recreated. They used density-functional theory (DFT) to calculate the band structure of Hexagonal boron nitride (h-BN).

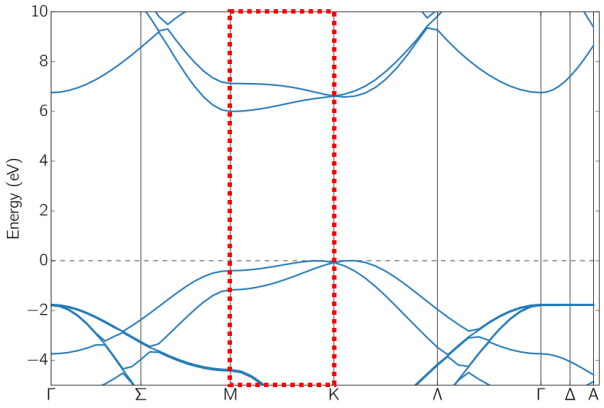

Figure 13: The calculated band structure from Schuster et al. The MK direction, our area of interest, is marked with a red box.

The band structure is presented in Figure 13. The data was acquired by sampling point from this image. To increase the data size cubic splines was fitted to each band separately. Then, using a linearly spaced k-point range new points where interpolated. This does not evade the inherent problem of state distribution, since there is obviously not enough information to recreate the density of state from simply this image. The band located in the lower right corner has also not been included in calculations as it also seems to be missing from the Schuster et al. JDOS. A comparison of the two computed JDOS plots is presented in Figure 14. The two images are quite different, but there are some similarities. Following the white/gray lines, we see that they trace out the area of high intensity of the Schuster et al. JDOS. Both agree on an indirect band gap at a little over $E_g \approx 6$ eV, corresponding to a momentum transfer of $|q| = 0.8$ Å^{-1}.

The elephant in the room is the spread of states in the ΔE direction, especially for higher momentum transitions. There can be a multitude of reasons for this. Firstly setting energy and momentum bin sizes impacts how smeared the JDOS becomes (see the comparison of Figure 5 and Figure 6). Actual EELS experiments often have relatively large momentum uncertainties (for instance [7] at $\delta q \approx 0.25$ Å^{-1}) and it is probable that Schuster et al. have calculation to more closely match experiments. Unfortunately this is infeasible for our approach, due to the linear spacing of k-points in the band structures. Making bin sizes too large will overwhelmingly count small $|q|$ (making the points in Figure 2 left more sparse), and can be problematic when identifying indirect band gaps at larger momentum transfers. In addition, we have only sampled k-points from $M - K$. If the whole Brillouin zone was available, we would prefer to sample every q transition parallel to $M - K$. Unfortunately to achieve this, a full DFT simulation is required.

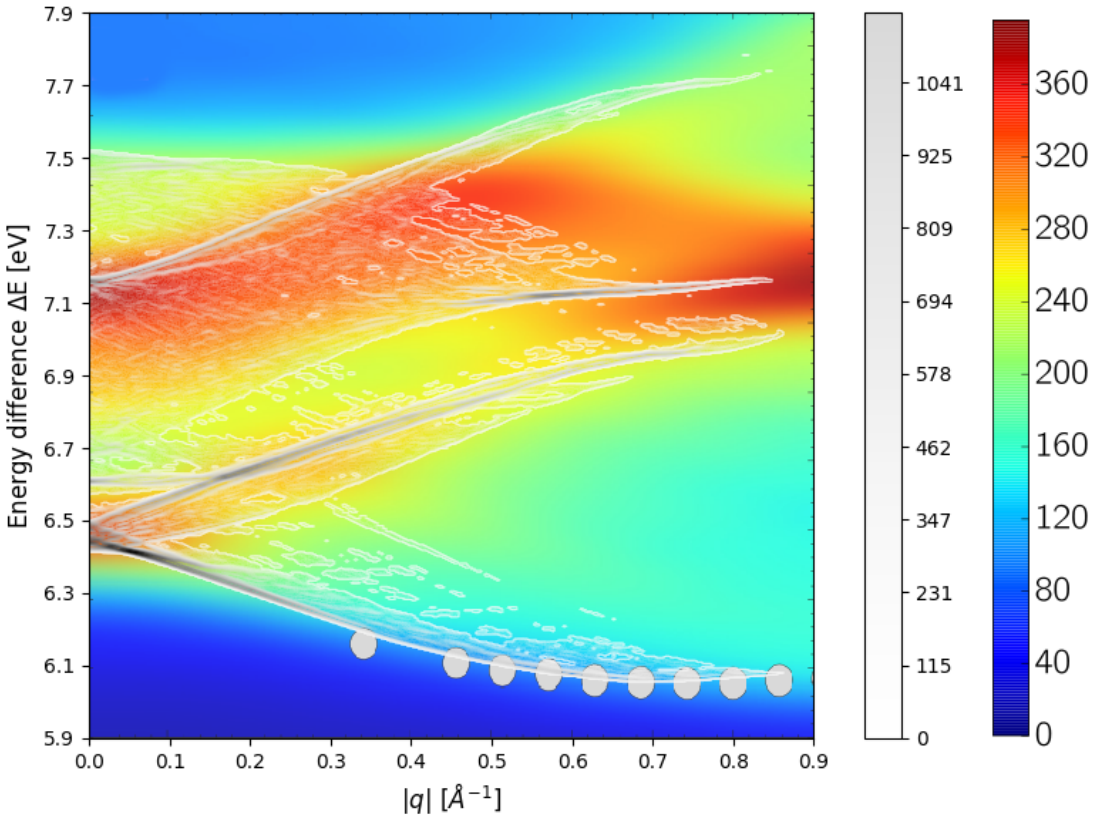

Figure 14: Showing two different JDOS calculations from the MK direction of the band structure from Figure 13. The blue to red density plot is from Schuster et al. while the gray overlaying density is calculated from the method presented here.

4 Experimental

We will now analyse spectrums measured by an electron microscope at different momentum transfers. By accelerating electrons with a narrow energy range, these can be pointed at a thin sample. Inbound electrons will interact with the sample by a number of different mechanisms. Measuring the energy of the outgoing electrons, one can calculate the electron energy loss after passing through the sample. Using a strong magnetic field (magnetic prism) the outgoing electrons can be separated as a function of their energies, thus giving the intensities of electrons at different energy losses. The interaction between the inbound electrons and sample undergoes two types of scattering, *elastic* and *inelastic*.

Elastic scattered electrons, often called forward scattered, corresponds to electrons that interact with the sample in such a way that the outgoing electrons have no energy loss. In the energy loss spectrum this will be a sharp intensity peak centred at 0, with a spread corresponding to the energy spread of the incident beam, appropriately named the zero loss peak (ZLP). The ZLP should be extracted from the spectrum, where the first width half maximum (FWHM) often is used as the energy resolution of the spectrum. For all spectrums shown here, the ZLP has been removed by Phuong Dan Nguyen (thank you).

Inelastic scattered electrons corresponds to electrons that loose energy after passing through the sample. The cause of inelastic scattering is attributed to more than a hand-full of effects such as phonon excitation, plasmon excitation, Cherenkov radiation, band transitions and more. Among these we will be interested in determining the band gap as previously discussed.

Momentum resolution can be achieved since momentum transfer is dependent on the scattering angle [8]. By moving the spectrometer entrance aperture one can single out what scattering angles to measure. Measuring a series of angles, on allows to get multiple energy spectrums corresponding to different momentum transfers.

Approximating both the VB and CB as parabolic, the 3-dimensional JDOS for a direct band gap integrated over all q values [9] is proportional to

$$JDOS \propto \sqrt{E - E_g} \tag{12}$$

This neglects some of the complications previously presented and a care full selection of fitting ranges (which energy range of the spectrum to fit) must be preformed. At higher q-values the direct band gap can not be measured by the microscope. For

these values, the band gap (E_g) of (12) will not correspond to the lowest possible energy transition over all q, but rather the lowest energy transition of in a specific q-range. Thus as the CB increases in energy for higher q-transitions we will expect the fitted E_g value to also increase. Due to the shape of the proportionality of JDOS, the fitted energy range has to be above the E_g value. To find these ranges assistant from DFT calculations came in handy (see next section). After the fits were done we should also compare with values from the DFT calculations.

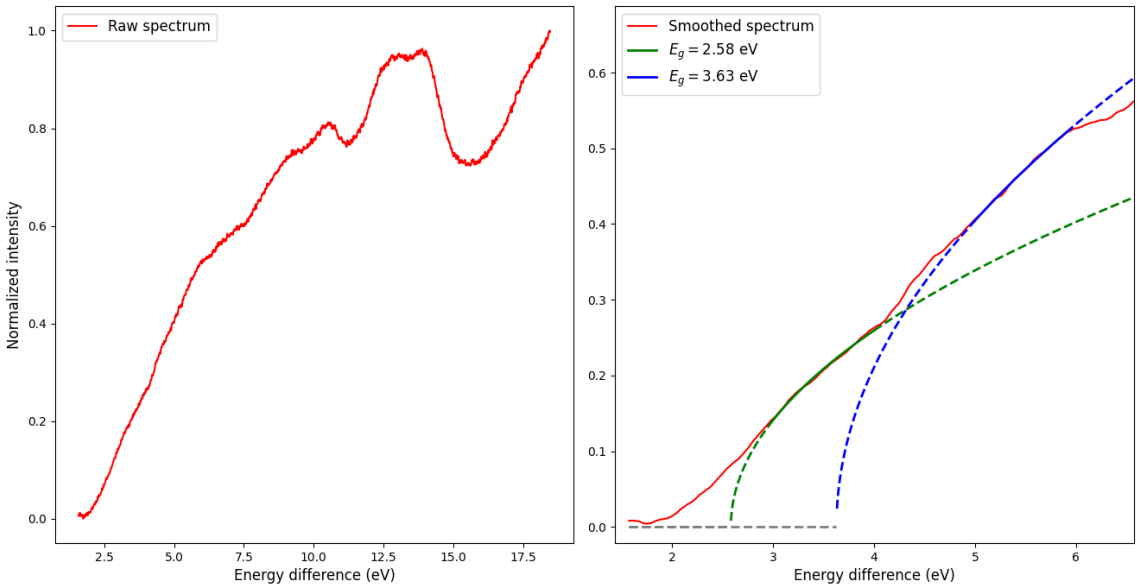

Figure 15: Left: Intensity spectrum as a function of energy difference for $q \in \{0, 0.1\}$ Å^{-1}. Right: The same spectrum smoothed for easier fitting of $\sqrt{E - E_g}$. Two different regions are fitted, in green (3.00 eV, 4.00 eV) and in blue (4.70 eV, 5.50 eV), illustrating that the determined band gap is highly dependent on energy range chosen to preform the fit.

5 Materials Project

From the Materials Project (MP) [10], DFT calculated band structures can be extracted for a numerous amount of different materials. Trough the `pymatgen`-API [11] energies and k-points along high-symmetry lines in the Brillouin zone can extracted. This will not mediate the problem of points becoming more sparse for higher q transitions (see Figure 2) as MP does not store energies trough the whole Brillouin zone. The k-points connecting the high symmetry points are very sparse, so cubic spline interpolation has been used to increase the k-point density. It should be noted that DFT underestimates the true band gap of materials [12]. This however can be solved by a applying a scissor operator, shifting the energy difference between the VBM and CBM to fit experimental data.

The DFT calculated data from MP is given in fractional coordinates. This means that coordinates are given as fractions of the Brillouin Zone primitive vectors, and are thus unit-less. A general k-point in reciprocal space can the be expressed as.

$$\mathbf{k} = h\mathbf{a} + k\mathbf{b} + l\mathbf{c}$$

Where (h, k, l) are the unit-less fractional coordinates, which MP uses as a basis for its k-points. To transform these to Cartesian coordinates, we have to multiply the (h, k, l) fractional coordinates by a transformation matrix U give by [13][14].

$$U = \begin{pmatrix} a & b\cos\gamma & c\cos\beta \\ 0 & b\sin\gamma & c\frac{\cos\alpha - \cos\beta\cos\gamma}{\sin\gamma} \\ 0 & 0 & \frac{\Omega}{ab\sin\gamma} \end{pmatrix}$$

Where $a = |\mathbf{a}|$, $a = |\mathbf{b}|$ and $a = |\mathbf{c}|$ and α, β and γ are the angles between $(\mathbf{b}, \mathbf{c})$, $(\mathbf{a}, \mathbf{c})$ and $(\mathbf{b}, \mathbf{c})$ respectively. Here we have made use of Ω , the volume of the Brillouin Zone unit cell, given by.

$$\Omega = \mathbf{a} \cdot (\mathbf{b} \times \mathbf{c}) = abc\sqrt{1 - \cos^2\alpha - \cos^2\beta - \cos^2\gamma + 2\cos\alpha\cos\beta\cos\gamma}$$

We will investigate the structure of three different semi conductors. Firstly we look at Zinc oxide (ZnO). ZnO is a direct band gap material and has a hexagonal crystal structure. Secondly SnO_2(finn riktig variant). Finally we will look at 4H Silicon carbide (SiC), having a indirect band gap.

5.1 ZnO

We begin by looking at the JDOS for ZnO along the symmetry lines where the band gap is located. The Brillouin zone in addition the band structure is shown in Figure 16. As discussed, the bang gap has been adjusted using a scissors operator. From [15] the band gap of ZnO was found to be $E_g = 3.37$ eV and is the value used to adjust the DFT calculated structure. As seen in figure Figure 16, the band gap is located at the Γ point (it is a direct semi conductor after all),thus both the $K\Gamma$ and ΓA JDOS spectrums are calculated. To not have a too large energy spread, only the lowest energy CB was included in the calculations for both $K\Gamma$ and ΓA, while the 8 highest VBs were included. All bands were interpolated with 1500 points each. This number was found to be reasonable since it was enough to capture the main features while still being computationally feasible.

The two JDOS calculations are presented in Figure 17. The lowest energy transitions are correctly identified at $E_g = 3.37$ eV, corresponding to the energy shift following the use of a scissor operator. In the $K\Gamma$ direction, we observe that for negative q transitions the energy gap required increases quickly. This is due to CB growing quickly in energy when approaching the K point. It seems that due to the steepness of this CB, the shape of the VB is more arbitrary than that of the positive q transitions. For these positive q transitions, more features from higher q-values are distinguishable, attributed to the flattening of the CB around the Γ point.

In the ΓA direction we see a splitting of two lines starting at $(-0.6\ \text{Å}^{-1}, 3.9\ \text{eV})$ and ending at $(0, 4.1\ \text{eV})/(0, 3.37\ \text{eV})$. These lines are attributed to transitions from the two high energy valence bands meeting at the A point to the CBM. Since the top line decreases in E when q goes to -0.6 Å^{-1}this belongs to transitions lower band, while the bottom line increases in E when q goes to -0.6 Å^{-1}, belonging to transitions from the higher band. The intensity difference is probably attributed to two main effects. Firstly the lower band is slightly flatter than the higher band, resulting in denser energy transitions (see discussion regarding Figure 10). In addition the "shadow" of the higher band (that is, transitions that does not go to the CBM) overlap with the $(-0.6\ \text{Å}^{-1}, 3.9\ \text{eV})$ to $(0, 4.1\ \text{eV})$ line, thus increasing the density of state.

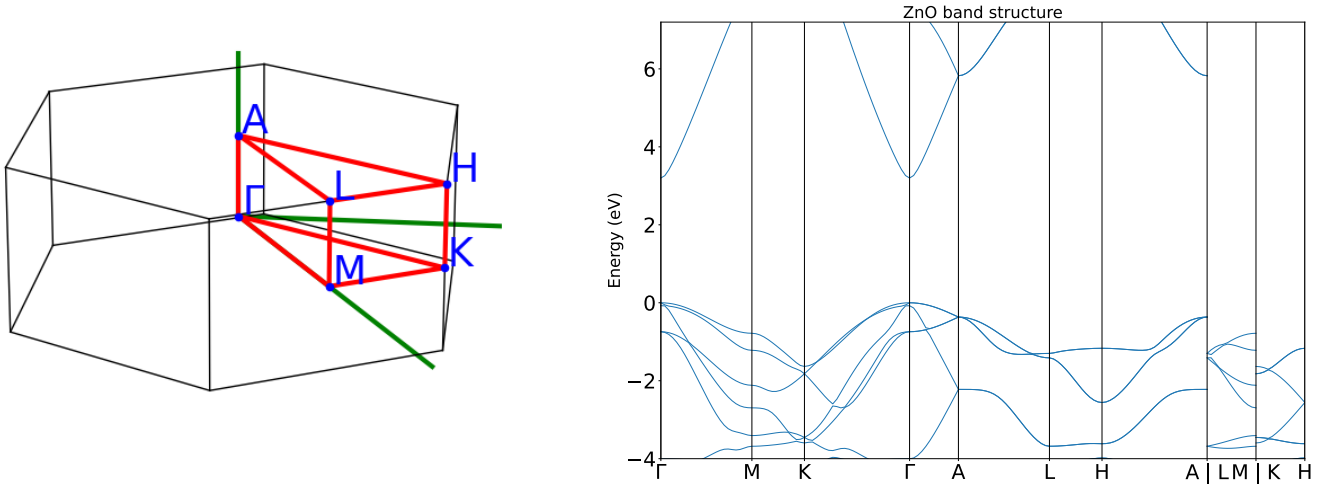

(a) Brillouin Zone

(b) Band structure

Figure 16: Left (a): Hexagonal Brillouin zone of ZnO. The three green lines represents the reciprocal lattice vector. High symmetry points are labeled by blue letters, with red lines tracing their paths. Right (b): The corresponding band structure of ZnO. Energy is plotted following the red symmetry lines (a). The direct band gap is located on the intersection $K\Gamma$, ΓA.

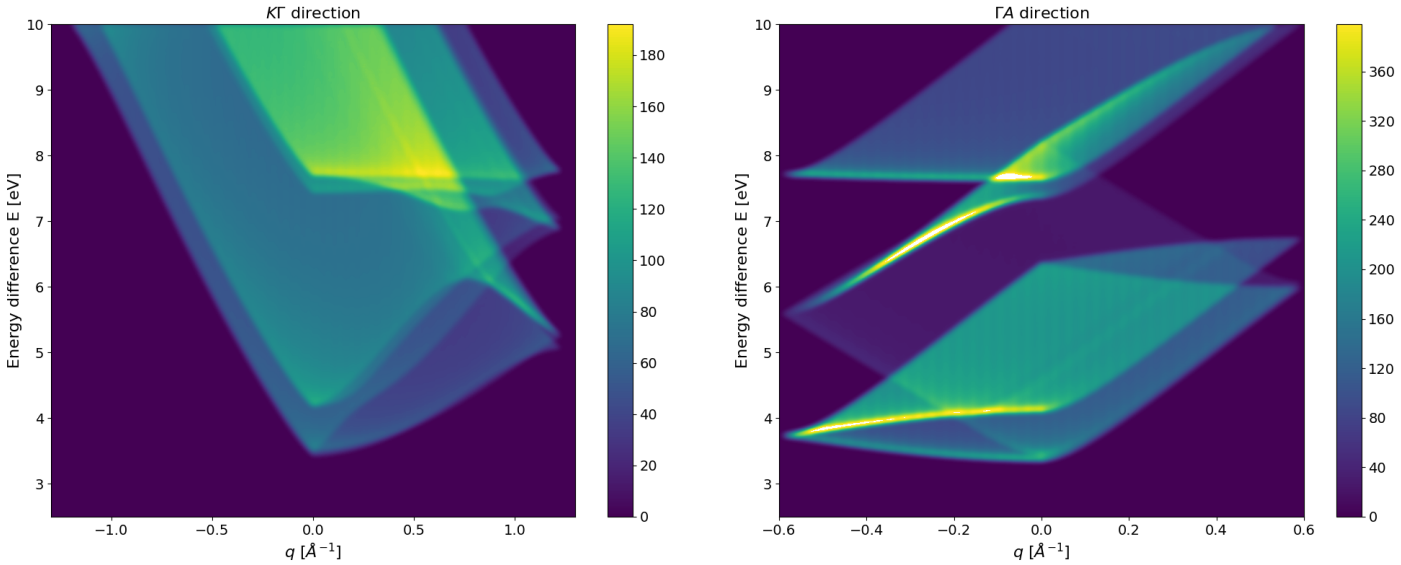

(a) $K\Gamma$ (b) ΓA

Figure 17: Left (a): JDOS plot of transitions in the $K\Gamma$ direction. The lowest energy CB (seen in Figure 16 (a)) and 8 of the lowest energy VBs was included. Energy and momentum bin sizes set at $\delta E = 1.5 \cdot 10^{-2}$ eV and $\delta q = 5.2 \cdot 10^{-3}$ Å^{-1}. Right (b): JDOS plot of transitions in the ΓA direction. The 2 lowest energy CBs and 7 highest energy VBs was included. Energy and momentum bin sizes set at $\delta E = 1.5 \cdot 10^{-2}$ eV and $\delta q = 2.4 \cdot 10^{-3}$ Å^{-1}.

5.2 SnO_2

References

[1] Charles Kittel. *Introduction to solid state physics*. eng. Hoboken, N.J, 2005.

[2] George Collins. *The virial theorem in stellar astrophysics*. Tucson: Pachart Pub. House, 1978. ISBN: 9780912918136.

[3] R. J Elliott. *An introduction to solid state physics and its applications*. eng. London, 1974.

[4] Harley Flanders. *Differential forms with applications to the physical sciences*. eng. New York, 1989.

[5] Christopher Gaul et al. "Insight into doping efficiency of organic semiconductors from the analysis of the density of states in n-doped C_{60} and ZnPc". In: *Nature Materials* 17 (2018), pp. 439–444. ISSN: 15. DOI: https://doi.org/10.1038/s41563-018-0030-8.

[6] R. Schuster et al. "Direct observation of the lowest indirect exciton state in the bulk of hexagonal boron nitride". In: *Physical Review B* 97.4 (2018). ISSN: 2469-9969. DOI: 10.1103/physrevb.97.041201. URL: http://dx.doi.org/10.1103/PhysRevB.97.041201.

[7] F. S. Hage et al. "Momentum- and space-resolved high-resolution electron energy loss spectroscopy of individual single-wall carbon nanotubes". In: *Phys. Rev. B* 95 (19 2017), p. 195411. DOI: 10.1103/PhysRevB.95.195411. URL: https://link.aps.org/doi/10.1103/PhysRevB.95.195411.

[8] F. S. Hage et al. "Topologically induced confinement of collective modes in multilayer graphene nanocones measured by momentum-resolved STEM-VEELS". In: *Phys. Rev. B* 88 (15 2013), p. 155408. DOI: 10.1103/PhysRevB.88.155408. URL: https://link.aps.org/doi/10.1103/PhysRevB.88.155408.

[9] B. Rafferty and L. M. Brown. "Direct and indirect transitions in the region of the band gap using electron-energy-loss spectroscopy". In: *Phys. Rev. B* 58 (16 1998), pp. 10326–10337. DOI: 10.1103/PhysRevB.58.10326. URL: https://link.aps.org/doi/10.1103/PhysRevB.58.10326.

[10] Anubhav Jain et al. "The Materials Project: A materials genome approach to accelerating materials innovation". In: *APL Materials* 1.1 (2013), p. 011002. ISSN: 2166532X. DOI: 10.1063/1.4812323. URL: http://link.aip.org/link/AMPADS/v1/i1/p011002/s1\&Agg=doi.

[11] Shyue Ping Ong et al. "Python Materials Genomics (pymatgen): A robust, open-source python library for materials analysis". In: *Computational Materials Science* 68 (2013), pp. 314–319. ISSN: 0927-0256. DOI: https://doi.org/10.1016/j.commatsci.2012.10.028. URL: https://www.sciencedirect.com/science/article/pii/S0927025612006295.

[12] John P. Perdew et al. "Understanding band gaps of solids in generalized Kohn–Sham theory". In: *Proceedings of the National Academy of Sciences* 114.11 (2017), 2801–2806. ISSN: 1091-6490. DOI: 10.1073/pnas.1621352114. URL: http://dx.doi.org/10.1073/pnas.1621352114.

[13] J. L. Sussman et al. "A structure-factor least-squares refinement procedure for macromolecular structures using constrained and restrained parameters". In: *Acta Crystallographica Section A* 33.5 (1977), pp. 800–804. DOI: https://doi.org/10.1107/S0567739477001958. eprint: https://onlinelibrary.wiley.com/doi/pdf/10.1107/S0567739477001958. URL: https://onlinelibrary.wiley.com/doi/abs/10.1107/S0567739477001958.

[14] M. G. Rossmann and D. M. Blow. "The detection of sub-units within the crystallographic asymmetric unit". In: *Acta Crystallographica* 15.1 (1962), pp. 24–31. DOI: https://doi.org/10.1107/S0365110X62000067. eprint: https://onlinelibrary.wiley.com/doi/pdf/10.1107/S0365110X62000067. URL: https://onlinelibrary.wiley.com/doi/abs/10.1107/S0365110X62000067.

[15] Norlida Kamarulzaman, Muhd Firdaus Kasim, and Roshidah Rusdi. "Band Gap Narrowing and Widening of ZnO Nanostructures and Doped Materials". In: *Nanoscale Research Letters* 10.1 (2015), p. 346. ISSN: 1556-276X. DOI: 10.1186/s11671-015-1034-9. URL: https://doi.org/10.1186/s11671-015-1034-9.